SSRG International Journal of Electrical and Electronics Engineering
ISSN: 2348-8379/ https://doi.org/10.14445/23488379/IJEEE-V13I3P115

Volume 13 Issue 3, 200-209, March 2026

Original Article

UWB Monostatic RADAR-Based Heartbeat Monitoring in an Autonomous Vehicle

Udhyami M B[1], Joseph Rodrigues[2]

[1,2]*Department of Electrical and Electronics Engineering, Christ Deemed to be University, Bangalore, India*

[1]*Corresponding Author : udhyami.mb@res.christuniversity.in*

Received: 11 December 2025 Revised: 14 January 2026 Accepted: 21 February 2026 Published: 31 March 2026

Abstract - *Monitoring a driver's physiological state in real time is vital for enhancing road safety by detecting fatigue, medical emergencies, and enabling future health-intervention systems in autonomous vehicles. Ultra-Wideband (UWB) impulse radio monostatic Radar emerges as an attractive alternative due to its ability to perform non-invasive and highly sensitive detection of vital signs, including respiration and heart rate, through obstacles such as clothing or car seats. This paper presents a radar setup located in the seat, which propagates a UWB signal through human tissues from the back side of the driver up to the heart location. The transmitted and reflected UWB signal and antenna reflection coefficient S11 parameter are analysed to detect the heart rate for a heartbeat-induced heart model. Various UWB pulse types and their spectral characteristics are analysed to ensure efficient energy transmission within the FCC mask safety constraints. Time-domain analysis of the transmitted and received pulses reveals clear heartbeat analysis with minimal distortion, achieving accurate heart detection rates. Reflected-pulse analysis shows clear differences in amplitude between systole and diastole for normal and abnormal heart-radius conditions, allowing reliable detection of heart states. Time-of-flight and range estimation help in tracking the heart-wall movement accurately. FFT-based analysis of the time-varying S11 parameter estimates the heart rate, confirming precise non-invasive heartbeat detection through the thorax.*

Keywords - *UWB Propagation, UWB Monostatic Radar, Non-Invasive Heartbeat Detection, Scattering Parameter, Vehicular Communication.*

1. Introduction

Ultra-Wideband (UWB) technology is a radio communication technology that operates over a wide range of frequencies. A low power spectral density can allow for a high temporal resolution, which reduces interference with other narrowband systems. UWB pulses are of short duration, hence suitable for detecting subtle movements [1]. These characteristics of UWB have led to increased adoption of UWB systems. UWB can be used for applications related to healthcare, particularly in environments where traditional methods may have limitations due to motion constraints and the need for vital sign monitoring. The technology also adheres to the FCC regulations regarding exposure to the human body, which ensure safety during long-term use [2].

UWB can propagate through human tissues, and after transmission, reflection can take place at internal organs. The vital parameters can be extracted from the reflected pulse [3], and the accuracy increases as it is placed close to the body [4]. A filter can be applied to reduce the noise and clutter [5], and multiple stationary object detection can occur during UWB radar [6]. From research, it is identified that UWB pulse exposure with low attenuation during transmission through the thorax makes it suitable for cardiovascular monitoring [7]. For continuous health monitoring, the UWB signal is becoming an emerging method nowadays. The implementation of UWB radar for respiration detection and heartbeat has been explored through various simulation-based and experimental approaches. Various simulation and experimental strategies can be implemented using UWB radar.

Vital parameter monitoring in a moving atmosphere is gaining prominence in applications for driver assistance and safety [8]. Feasibility of UWB impulse radar for the physiological studies. Recent studies validated the feasibility of using UWB impulse radar for vital sign monitoring due to its sensitivity and separated the micro-movements caused by internal organ activity. Vital sign detection, specifically for measuring heartbeat rate, is essential for early detection of medical emergencies, such as cardiac arrest [9]. UWB's ability to detect and monitor these parameters non-invasively makes it suitable for a range of applications, including elderly care, hospitals, and driver safety in vehicles. Contactless measurement of the driver's heartbeat rate through materials such as cloth and seat cover fabric in the vehicular atmosphere, UWB monostatic radar offers an effective

solution [10]. Multiple human target detection and interference from other moving organs' signals [11] can be determined using UWB radar. Consideration of artifacts due to body motion and overlapping of other vital signals is advisory in noncontact vital signal detection [12]. Multiple IR UWB Radar algorithms for multisensory data and Singular Spectrum Analysis (SSA) are proposed for multisensory data [13] and the short distance estimation with IR UWB [14].

Several studies emphasize the importance of pulse shape in UWB vital-sign detection [15, 16]. Several studies emphasize the importance of pulse shape in UWB vital-sign detection. Analytical studies show that the harmonic content can separate respiration and heartbeat, and propose filters to cancel respiration harmonics that mask the cardiac component [17]. Cardiac motion tracking using sub-nanosecond IR-UWB pulses has been demonstrated, relying on a wide bandwidth to resolve small chest displacements and to achieve accurate results [18]. Through-wall detection under low Signal-to-Noise Ratio (SNR) has been improved by designing pulses and processing schemes that isolate vital signals from clutter via spectral accumulation [19].

An optimal central frequency for monocycle pulses to enhance the reflected amplitude of chest-wall motion, emphasizing that centre frequency alignment is important as well as bandwidth [20]. Gaussian pulse's seventh-derivative offers sharp band control for better harmonic discrimination, good bandwidth for high-resolution motion detection, and the ability to be shaped for FCC mask compliance, allowing maximum permissible transmission power while preserving spectral efficiency [21]. Vital sign information of multiple targets with high accuracy in short distances [22], automotive system applications [23], shorter detection time, and less radiation [24] are also characteristics of UWB.

Various pulse propagation and return signals provide information on optimal RADAR and antenna configurations. The use of matched filters [25], envelope detection [26], and autocorrelation techniques [27] enhances signal processing accuracy [28]. The proposed work provides a detailed evaluation of a 7th-derivative Gaussian pulse designed to meet the FCC mask and optimized for in-vehicle heartbeat detection through seat and human-tissue layers. This study simulates reflection coefficient changes caused by heartbeat to show that heart rate can be accurately detected using phase-based analysis [29]. Thus, the overall contributions of this paper include:

- Employing a seventh-derivative UWB Gaussian pulse complying with the FCC spectral mask for transmission through multilayer thoracic tissues for the detection of human heart rate parameters.
- UWB monostatic Radar setup for continuous cardiac monitoring during driving conditions
- A realistic thorax model implemented in CST Studio Suite, incorporating dielectric property variations under normal and abnormal systolic and diastolic conditions.
- Distance estimation using Time-of-Flight analysis to track ventricular systole and diastole states.
- Phase-based analysis of the antenna reflection coefficient for heartbeat estimation in beats per minute.

The rest of the paper is organized as follows: Section II presents the theoretical background of Gaussian pulse generation, higher-order derivatives, FCC spectral mask, electrical properties of the thorax phantom, and the basic movements of the human heart. In Section III, antenna placement strategies and simulation setup are described. In Section IV, the results and discussion are provided, including time and frequency domain analysis of a Gaussian pulse and evaluation of the 7th derivative fitting within the FCC spectral mask. The estimation of cardiac displacement using reflection-based distance measurement and heartbeat estimation using FFT are also discussed. Finally, Section V concludes the paper with its suitability for Biomedical UWB sensing and possible directions for future research.

2. UWB Pulse Propagation for Non-Invasive Cardiac Monitoring

Several heart-rate detection methods have been reported for different applications. In vehicular environments, ECG-based monitoring techniques [8] suffer from significant limitations, as they require direct contact with the body, are highly affected by motion artifacts, and are uncomfortable and impractical for long-term use. Camera-based or PPG-based monitoring methods [9] face visibility issues due to poor or unavailable lighting at night and are strongly affected by occlusion and body motion. In addition, these optical techniques cannot penetrate clothing or seat materials, limiting their applicability for noncontact monitoring. Doppler radar-based approach has a continuous wave experience with limited range resolution, signal interface, and less accuracy under vehicular atmosphere. The selection of the UWB Gaussian pulse lower derivative does not comply with the FCC spectral mask. Thereby restricting transmitting power and penetration depth. Amplitude-based detection methods further exhibit reduced sensitivity to subtle cardiac motion and are susceptible to attenuation and multipath effects in confined vehicle environments. A UWB Gaussian pulse is employed for signal transmission through the human body in the IR-UWB system, providing the required centre frequency and bandwidth [1]. The fundamental Gaussian pulse is

$$x(t) = A * exp(\frac{-t^2}{2\sigma^2}) \quad (1)$$

Where A is the amplitude in time, and σ is the width of the pulse. This waveform is smooth and decays rapidly, leading to a compact spectrum in the frequency domain. However, the base Gaussian function contains significant low-frequency energy that violates the FCC emission mask, making it unsuitable for direct use in UWB systems [30, 31].

To address this limitation, higher-order derivatives of the Gaussian function are employed. In this work, the transmitting antenna of the UWB radar system is excited by a seventh-derivative Gaussian pulse. Its n-th order derivative can be expressed using.

$$X^{(n)}(t) = \left(\frac{d^n}{dt^n}\right)[A * exp(\frac{-t^2}{2\sigma^2})] \quad (2)$$

For better spectral efficiency and to meet regulations for emission performance, compared to lower-order monopulse, higher-order derivatives have improved spectral characteristics and enhanced radiation power, which are suitable for subtle psychological signatures. The propagation of the seventh derivative Gaussian pulse through the thoracic region is strongly influenced by the multilayer tissue structure, each characterized by distinct dielectric properties and thicknesses. The impedance mismatch at successive boundaries, such as skin–fat, fat–muscle, muscle–bone, and bone–myocardium, determines transmission, reflection, and absorption of the UWB signal, thereby affecting the backscattered response.

Table 1. Electrical properties of the thorax phantom

Layer	Estimated Thickness (mm)	ε_r	σ (S/m)
Skin (dry)	~2 – 3	~35 – 40	1.0 – 1.5
Subcutaneous Fat	~10 – 15	~5 – 7	0.05-0.1
Muscle (Chest Wall)	~15 – 20	~50 – 55	1.5 – 1.9
Rib / Bone	~5	~12 – 20	0.2 – 0.5
Heart (Myocardium)	~8 – 12	~58 – 60	1.8 – 2.0

Cardiac movement generates an additional time-varying component. The ventricular myocardium exhibits periodic changes in radius due to the diastolic relaxation as well as the systolic contraction phases. These resulting dimensional changes produce a subtle modulation of the effective dielectric boundary. When the radius decreases during systole, the curvature of the myocardium increases to locate variation in scattering corresponding to a shift in the amplitude and phase of the reflected pulse. At the diastolic condition, the radius increases, which modifies the propagation path length and reflection coefficient. Using the Monostatic antenna, these variations in the reflected waveforms can be monitored. When the permittivity is approximately 58-60, and the conductivity is between 1.8-2 S/m, which can be considered as relatively high conductivity and permittivity [32], which ensures strong electromagnetic interaction to detect cardiac motion.The rib and bone structure has relatively lower permittivity and transparency to UWB frequencies. Modulation in the received signal generated from the cardiac layers to confirm the radius-based vital parameter detection and viability. Table 1 presents the electromagnetic and structural properties of human thoracic tissues, such as skin, fat, muscle, rib/bone, and heart myocardium. It summarises how each layer interacts with electromagnetic waves, which is critical for understanding and analysing the backscattered signals used for detecting heart motion or other vital parameters [33]. The human heart consists of four main chambers: the Left Ventricle (LV), Right Ventricle (RV), Left Atrium (LA), and Right Atrium (RA). Among these, the moving parts are the left ventricular wall, interventricular septum, and the cardiac valves—mitral, tricuspid, aortic, and pulmonary—play crucial roles in cardiac function.

The most dynamic structures are the LV and RV walls, particularly the left ventricular free wall and the interventricular septum, which exhibit significant movement during the cardiac cycle and are essential for effective pumping action [34]. In the proposed method, human tissue interaction with the UWB Gaussian pulse is studied, transmitted from the monostatic antenna. Moreover, the echo pulse is modulated by the motion induced by the cardiac boundary. FFT- based analysis, which enables heart rate estimation from these variations.

In the proposed work, the left ventricular free wall is considered the moving part of the heart. For the left ventricle, when the radius varies, the dielectric properties also vary in normal and abnormal heartbeat conditions. By measuring relative permittivity, ε_r, and conductivity, σ, heart radius changes can also be identified [35]. In abnormal states, the radius spans an expanded range and shows a progressive decrease in ε_r and σ, which reflects weakened contraction and altered electrical behaviour of the myocardium. In the normal cardiac motion condition, a smaller systolic radius produces higher permittivity and lower conductivity. In abnormal states, the radius spans an expanded range and shows a progressive decrease in ε_r and σ, which reflects weakened contraction and altered electrical behavior of the myocardium.

2.1. UWB Monostatic RADAR Setup for Heartbeat Monitoring

Figure 1 illustrates the proposed UWB Radar monitoring system block diagram for heartbeat monitoring. A UWB Gaussian seventh derivative pulse is transmitted through the Vivaldi antenna and propagates through different layers, finally, interacting with the heart model. A reflected pulse is generated from the transmitted pulse after hitting the dynamic heart. The reflected pulse transmits through the same medium of layers and is absorbed by the same monostatic antenna. From the reflected pulse by FFT-based analysis, an accurate estimation of heart rate in beats per minute can be made. The proposed work adopts a simulation-based approach using CST Studio Suite, where a realistic human environment is modeled by incorporating the dielectric properties of human tissues. A higher-order Gaussian pulse is employed to detect micro-displacement effects. The proposed simulation framework is

used for pulse propagation, antenna design, and tissue layer dielectric property study and validation to provide pulse selection criteria.

This method offers new insights into cardiac motion sensitivity and FCC-compliant higher-order Gaussian pulse behaviour.

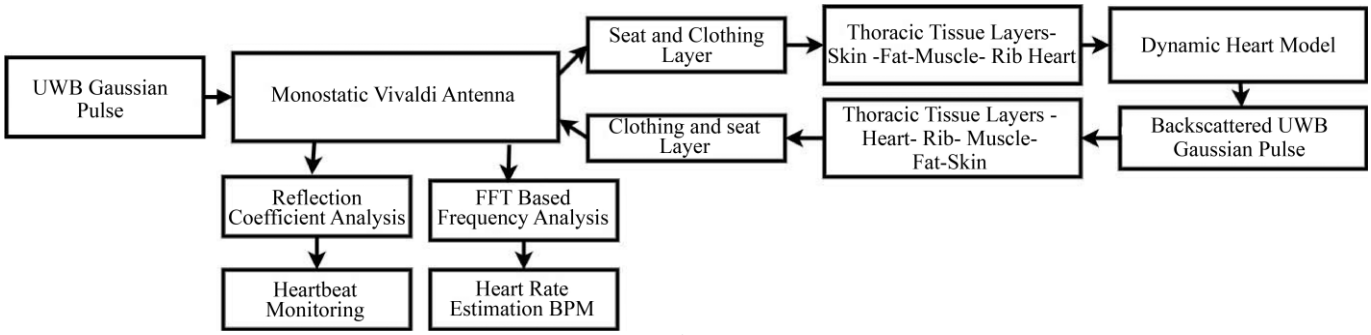

Fig. 1 Block diagram of UWB monostatic radar

In the proposed setup, the antenna is positioned at the back side at an approximate distance of 3 cm from the heart region of the Gustav voxel model in Computer Simulation Technology, CST Studio Suite, as shown in Figure 2, ensuring optimal coupling of UWB energy into the thoracic tissues. This close placement maximises the Signal-To-Noise Ratio (SNR) of the received backscatter.

The monostatic UWB radar system is simulated in CST Studio Suite, as shown in Figure 3. The Vivaldi antenna is excited through a discrete port with the seventh derivative Gaussian pulse, which propagates through seat, cloth, and multilayer biological tissues, which impinges on the dynamic heart model. The heart is parameterised with a time-varying radius to emulate periodic cardiac mechanical displacement. Variations in the radius of the moving part of the heart modulate the phase and amplitude of the backscattered UWB pulses, producing measurable changes in the reflected voltage waveform at the receiving port. By analysing these temporal variations in the received signal, heartbeat periodicity and corresponding vital sign information are accurately extracted.

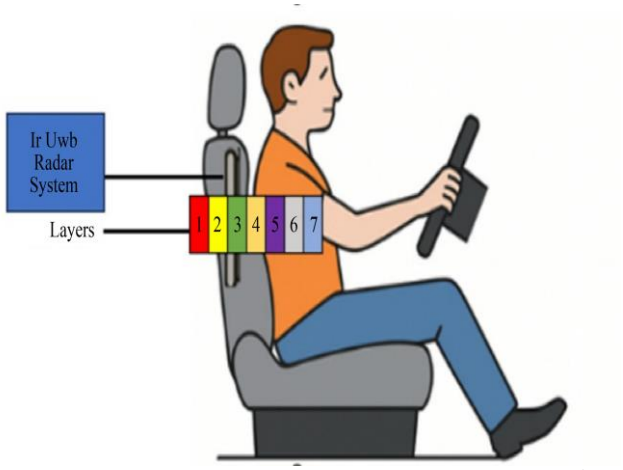

Fig. 2 Vital-Sign monitoring system through the posterior thorax for heart-rate detection across different layers: 1. Seat cover, 2. Clothing, 3. Skin, 4. Fat, 5. Muscle, 6. Rib and 7. Heart.

2.2. Heartbeat Measurement Employing UWB pulse

The motion of the heart is assessed by estimating the variation in distance between the radar sensor and the heart wall [36]. The transmitted UWB pulse reflects from the chest, and the returned signals corresponding to the systolic and diastolic phases exhibit slight differences in propagation delay. Delays can convert into distance for detecting subtle displacement due to heart contractions. By the FFT cross-correlation technique, the distance estimation can be carried out [14]. Without direct contact with the body, the distance between systolic and diastolic movement can be estimated.

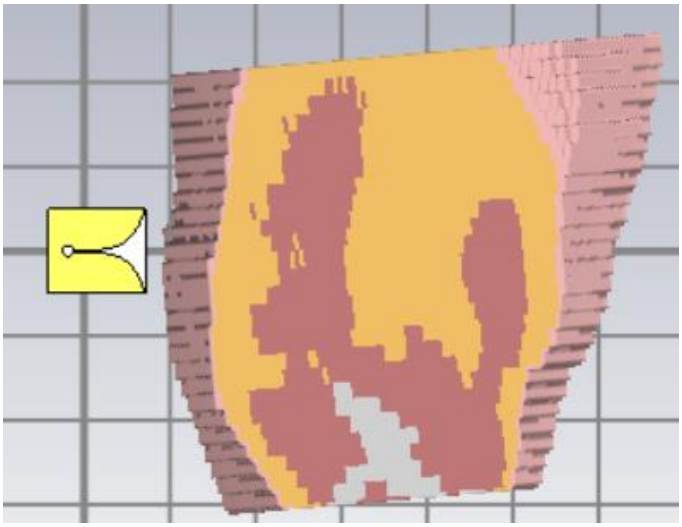

Fig. 3 CST simulation setup with vivaldi antenna for monitoring heart rate employing uwb gaussian pulse

When the UWB pulse interacts with thoracic tissues, the systolic and diastolic phases slightly modify the effective dielectric boundary, producing small but measurable changes in the reflected electromagnetic signal. These changes produce amplitude variations in S11, with the phase component being particularly sensitive to the mechanical displacement of the ventricular wall. The heartbeat is monitored by analysing the S11 signal generated by periodic

cardiac motions. To model this, two reflection states representing diastolic, $S_{11}^{\text{high}}$and systolic, S_{11}^{low} conditions are interpolated using a sinusoidal modulation at a specific heartbeat frequency, thereby reconstructing the time-domain evolution of the reflection coefficient. The resulting time-varying complex reflection coefficient is expressed as:

$$S_{11}(t) = (1 - m(t))\, S_{11}^{\text{low}} + m(t)\, S_{11}^{\text{high}} \quad (3)$$

Where

$$m(t) = 0.5[1 + \sin(2\pi f_{\text{hb}} t)] \quad (4)$$

Represents the heartbeat-induced modulation factor, and fhb is the heartbeat frequency in Hz. The fluctuations in magnitude and phase of S_11 (t)capture the electromagnetic effects of ventricular contraction and relaxation. To estimate the heart rate, the time-domain signal is transformed into the frequency domain using the Fast Fourier Transform (FFT), and the spectral frequency corresponding to the peak amplitude is identified. The heartbeat in Beats Per Minute (BPM) is then calculated as $f_{\text{peak}} \times 60$ [27].

3. Results and Discussion

A UWB Radar–based heart movement detection and estimation system is implemented using a seventh-derivative Gaussian pulse to excite the transmitter antenna of the monostatic UWB radar. The Gaussian pulse and its higher-order derivatives, i.e., first, fourth, sixth, and seventh, are analysed in time and frequency domains as in Figures 4 and 5 to assess their suitability for UWB-based heart rate estimation. Higher-order derivatives show more oscillations, zero crossings, and improved localization, which helps in capturing subtle movements. Spectral analysis indicates that increasing the derivative order reduces low-frequency energy and shifts power toward mid and high-frequency ranges, resulting in a wider bandwidth and lower spectral leakage. A sharp pulse is obtained by employing the proposed pulse with a centre frequency of 5.1 GHz and a pulse width of 1 ns. The seventh derivative, in particular, meets FCC UWB limits while maintaining spectral occupancy. Compared with the 1st and 4th derivative pulses, the 7th derivative pulse shows a higher zero crossing rate, a higher spectral centroid, and better temporal localization, while still keeping the oscillatory behaviour in control. Because of this, the seventh derivative gives more sensitivity to the dielectric boundary changes caused by cardiac contraction.

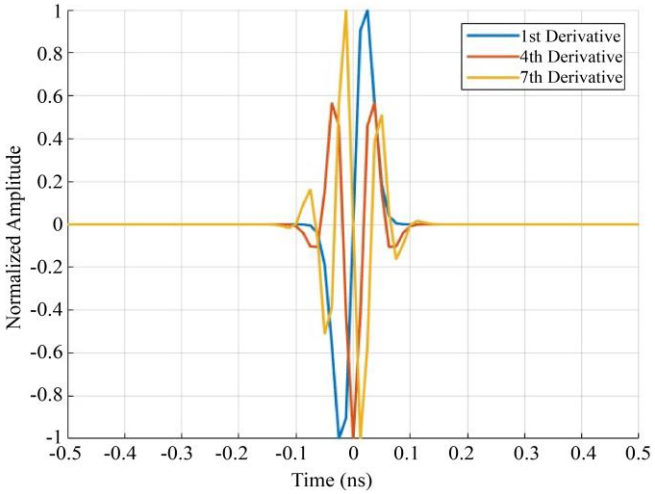

Fig. 4 Gaussian pulse first, fourth, and seventh derivatives in the time domain

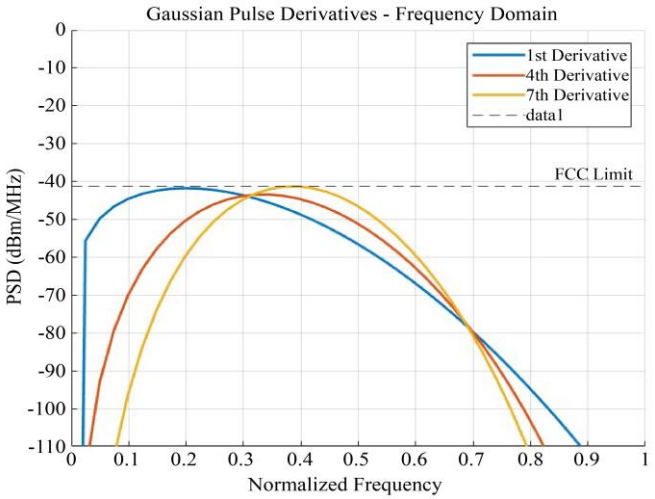

Fig. 5 Spectral mask of FCC and PSD of gaussian first, fourth, and seventh pulse derivative in the frequency band of 3.1 to 10.6 GHz

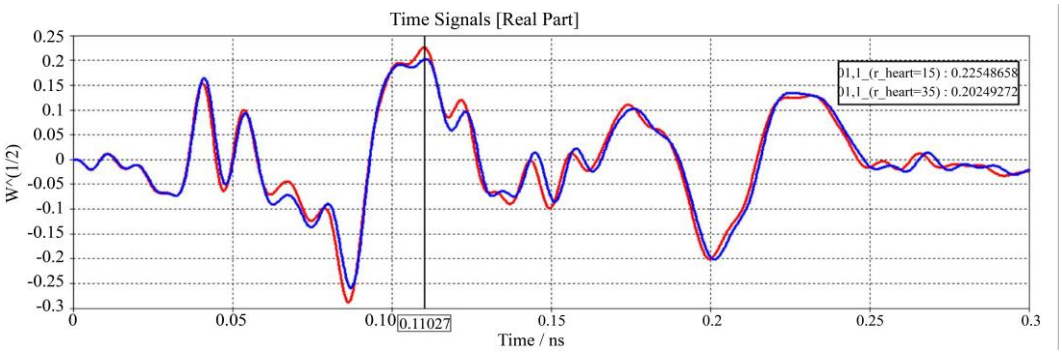

Fig. 6 Amplitude variations of backscattered UWB RADAR signals for heart radii of 15mm and 35 mm

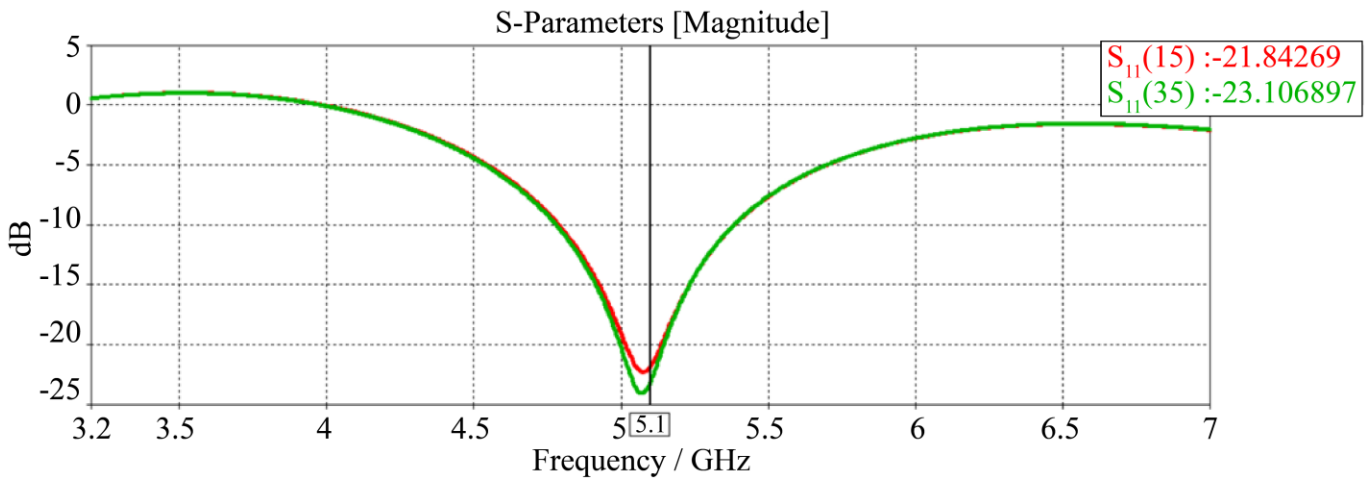

Fig. 7 S11 Plot of the monostatic UWB radar, excited by the seventh-derivative gaussian UWB pulse for heart radii of 15 mm and 35 mm

On the other hand, derivative orders more than seven introduce more oscillations and spread the energy in the time domain. This can reduce the propagation efficiency in multilayer biological tissues due to cumulative attenuation and phase distortion effects. The seventh derivative can be considered as the maximum suitable order, since it improves temporal sharpness without causing too much ringing or energy loss. This makes the seventh-order Gaussian derivative particularly effective for capturing subtle thoracic micro-movements required for non-invasive UWB-based vital parameter detection. The PSD matches the FCC emission. From the simulation studies carried out, Table 2 shows the obtained reflected pulse characteristics of the heart at different radii corresponding to cardiac phases, such as diastole and systole. The parameters include the relative permittivity, the conductivity of the heart tissue, and the peak voltage of the reflected signal. As the heart radius changes with contraction and relaxation, variations in ε_r and σ occur due to the dynamic dielectric properties of the heart tissue and blood volume. The reflected voltage is higher during the systole, while it is lower during diastole, indicating the physiological changes in heart wall thickness and blood distribution. Based on the different permittivity and conductivity values assigned for normal and abnormal diastolic and systolic conditions, the following results were obtained. For a normal heartbeat, the diastolic state of 25 mm radius produces a backscattered pulse peak.

Table 2. Peak voltage of the backscattered UWB Pulse under normal and abnormal heart-radius conditions

	Radius (mm)	Condition	ε_r	σ(S/m)	Vpeak
Normal	25 mm	Diastole	51.9	1.91	0.123635
	15 mm	Systole	58.2	1.85	0.263178
Abnormal	25 mm	Systole	58	1.80	0.179448
	35 mm	Diastole	56	1.60	0.132595

Amplitude of 0.123 V, while for a 15 mm radius, the peak increases to 0.263 V. In an abnormal condition, the systolic state of 25 mm radius shows a peak voltage of 0.179 V, and the diastolic state of 35 mm radius produces a peak voltage of 0.1325 V. By tracking the voltage variations across cycles, the periodicity of the heartbeat can be used to determine whether the heart is in systole or diastole. This indicates proper contractility of the heart and regular rhythmic activity. Figure 6 shows the amplitude variations of backscattered UWB signals for heart radii of 15 mm and 35 mm. From the graph, it is clear that the peak voltage differs between the systole and diastole conditions. Specifically, the signal corresponding to the larger heart radius of 35 mm exhibits a lower peak voltage of 0.2021 V during systole. The seventh-derivative Gaussian pulse provides the temporal resolution needed for reliable non-invasive cardiac motion detection. Figure 7 represents the scattering parameter plot of the monostatic UWB Radar, excited by the seventh-derivative Gaussian UWB pulse for a heart with radii of 15 mm and 35 mm.

Simulation evaluation demonstrates that the system achieves highly accurate range estimation. The distance is calculated using $(c \times \tau)/2$ [12], where τ is the measured time delay and c is the speed of light. As tabulated in Table 3, for a heart of 15 mm radius, the estimated distance between the antenna and the heart wall is 3.82 mm, which closely matches the actual distance of 4 mm. Similarly, for a radius of 25 mm, the estimated distance is 3.10 mm, where the actual distance is 3 mm.

Figure 8 shows the transmitted and received UWB radar pulse for heart radii of 15mm and 25 mm with magnitude and phase delay. These results confirm that the UWB radar, combined with time-of-flight analysis, can reliably trace the

physiological movement of the heart wall and assess normal or abnormal cardiac conditions based on deviations in the detected radius and motion pattern represented by the cross-correlation at corresponding stages, as shown in Figure 9.

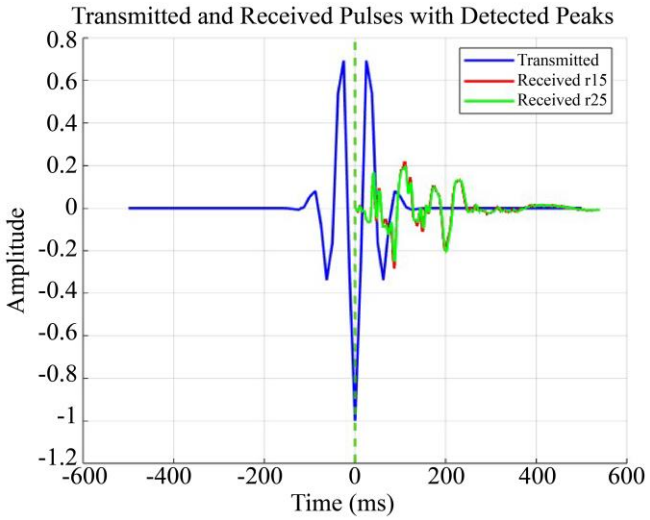

Fig. 8 Transmitted and received UWB RADAR pulse for heart radii of 15mm and 25 mm

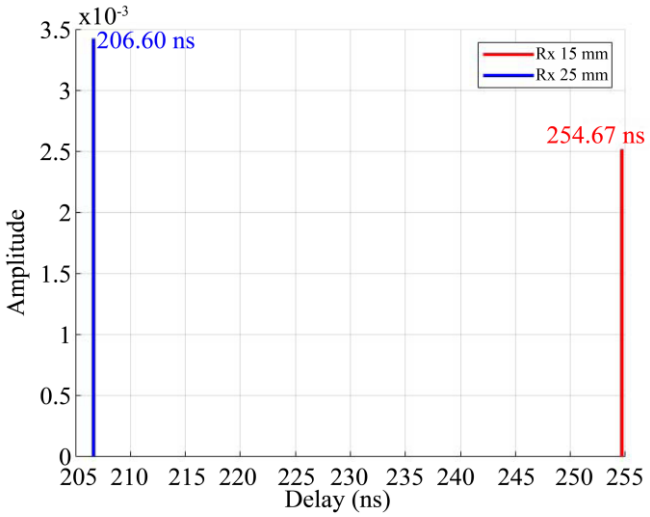

Fig. 9 FFT of UWB radar reflected heartbeat signal for 15 mm and 25 mm heart radii for estimating the pulse propagation delay

The heartbeat estimation detection model is implemented by loading two CST Studio Suite measured reflection coefficient datasets representing different cardiac states, corresponding to two distinct heart radii of 15 mm and 25 mm. To replicate the periodic expansion at a selected mid-band frequency point, enabling smooth interpolation between the low-radius and high-radius S11 responses.

Due to this modulation, which produces the change in electromagnetic properties by real cardiac motion. Due to this, the S11 sequence can also be viewed with noticeable changes, and it can be decomposed into two components: magnitude and phase. Moreover, these magnitude and phase components can visualize the variations caused by the heart movement.

The measured fluctuations show the magnitude variation remains extremely small, as less than 0.1 dB. In contrast, the phase variation reaches approximately 1.2°, confirming that the phase of S11 is significantly more sensitive to subtle dielectric boundary changes produced by cardiac movement.

Table 3. Distance estimation between the radar and the heart wall using time of flight

Radius(mm)	Delay(ns)	Distance(cm)
15	254.67	3.82
25	206.67	3.10

The estimation of heartbeat rate from the S11 signal is carried out using FFT analysis. In FFT analysis, the frequency corresponding to the peak magnitude can be identified. From Figure 10(c), the resulting peak corresponds to the frequency. f_{peak} can estimate as 1.3 Hz. Moreover, the heartbeat can be found out using. f_{peak}×60 and the estimated heartbeat is 71.9 BPM. The estimated value closely matches the induced heartbeat model value of 72 BPM. A comparative examination of the magnitude response, phase response, and FFT results confirms that phase-based monitoring provides higher sensitivity to physiological motion, thereby making it well-suited for reliable noncontact heartbeat detection. Figure 10 (a)-(c) illustrates the simulated variations in magnitude and phase, along with the corresponding frequency spectrum over a 10-second observation interval, demonstrating the underlying detection process and the extracted cardiac frequency.

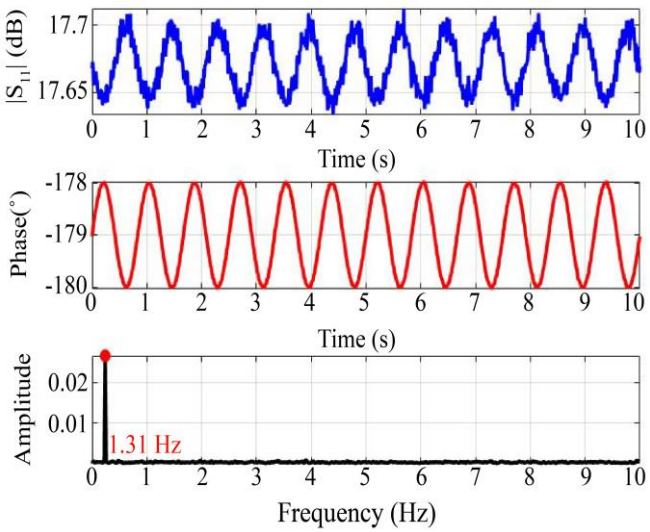

Fig. 10 Measurements of the reflection coefficient, S11, over a 10-second interval: (a) Magnitude in dB affected by heartbeat-induced variations, (b) Phase in degrees affected by Heartbeat-induced variations, and (c) Frequency spectrum with the corresponding frequency to the estimated heartbeat.

3.1. Result Validation

This section discusses the suggested algorithm with current methods for heartbeat estimation. The performance of Gaussian derivative pulses in terms of frequency, bandwidth, characteristics, FCC compliance, and cardiac motion sensitivity is summarized in Table 4. Due to narrow bandwidth and predominantly low-frequency components, the first-derivative Gaussian pulse has limited cardiac motion sensitivity and partial FCC compliance [15, 25]. Improved FCC compliance and moderate sensitivity result from the fourth-derivative Gaussian pulses with lower low-frequency and moderate bandwidth [16, 23]. The suggested UWB impulse radar-based strategy and current heartbeat monitoring techniques are mentioned in Table 5.

Although conventional ECG sensors have great heart rate accuracy and high motion sensitivity, their use in automotive settings is restricted because of their vulnerability to motion artifacts and the requirement for direct contact with existing heartbeat monitoring methodologies.

Due to their susceptibility to motion artifacts and requirement for direct contact with the subject, conventional ECG sensors have limited applicability in vehicle environments despite their high motion sensitivity and excellent heart rate accuracy [35].

Moderate motion sensitivity is provided by camera-based PPG techniques. However, they are unable to penetrate clothing or seating materials, and visual obstructions have a significant impact on their performance, leading to higher estimation errors [23]. Continuous-Wave (CW) Doppler radar systems exhibit moderate motion sensitivity and partial penetration through non-conductive materials.

However, phase noise and multipath effects cause accuracy to deteriorate in dynamic vehicular conditions [1, 16]. In contrast, the proposed 7th-derivative Gaussian pulse achieves full FCC compliance with wide bandwidth and sharp spectral confinement, providing higher reflected peak voltage and improved sensitivity to small cardiac displacements.

Table 4. Comparison of gaussian pulse derivatives for UWB-Based cardiac motion detection

Pulse Type	FCC Compliance	Bandwidth Characteristics	Peak Reflected Voltage	Cardiac Motion Sensitivity
1st-derivative Gaussian [15, 25]	Partial	Narrow bandwidth with low-frequency components	Low	Limited sensitivity
4th-derivative Gaussian [16, 23]	Improved	Moderate bandwidth with reduced low-frequency	Moderate	Moderate sensitivity
7th-derivative Gaussian (Proposed)	Full	Wide bandwidth with sharp FCC mask confinement	High	High sensitivity

Table 5. Comparison of the proposed UWB Radar approach with existing Vital-Sign monitoring techniques

Methodology	Penetration Through Seat/Clothing	Motion Sensitivity	In-Vehicle Suitability	Heart Rate Error
ECG sensors [35]	Not applicable	High	Limited due to sensitivity to motion artifacts	< 1%
Camera-based PPG [23]	No	Moderate	Limited due to lighting conditions and obstruction	2–5%
CW Doppler radar [1, 16]	Partial	Moderate	Moderate	1–3%
UWB IR (Proposed)	Yes	High	High	≈ 0.14%

4. Conclusion

This paper demonstrates the feasibility of using a UWB impulse radio monostatic RADAR system, supported by CST Studio Suite - based simulations, for noncontact and real-time detection of vital signs in vehicular environments. By employing higher-order Gaussian derivative pulses, particularly the seventh derivative, the system achieves both FCC compliance and high spectral efficiency, enabling precise monitoring of subtle cardiac motions through multilayer thoracic tissues.

The reflected pulse variations across normal and abnormal heart conditions highlight the radar's capability to distinguish physiological states, while the Vivaldi antenna. The design ensures reliable signal transmission and reception. The simulation successfully validates that phase-based monitoring of S11 variations, hence enables precise and reliable heartbeat detection with minimal estimation error. These results confirm that UWB radar offers a safe, efficient, and robust solution for in-vehicle health monitoring, and traditional contact-based sensing techniques are not suitable for continuous detection in a vehicular environment in dynamic vehicular settings. The S11 return loss parameters confirm proper antenna matching across the UWB band. Future work will focus on experimental validation with human subjects, advanced signal processing techniques for noise reduction, and integration into smart driver-assistance systems for enhanced road safety.

References

[1] Changzhi Li et al., "A Review on Recent Advances in Doppler Radar Sensors for Noncontact Healthcare Monitoring," *IEEE Transactions on Microwave Theory and Techniques*, vol. 61, no. 5, pp. 2046-2060, 2013. [CrossRef] [Google Scholar] [Publisher Link]

[2] Moe Z. Win, and Robert A. Scholtz, "Impulse Radio: How it Works," *IEEE Communications Letters*, vol. 2, no. 2, pp. 36-38, 2002. [CrossRef] [Google Scholar] [Publisher Link]

[3] Antonio Lazaro, David Girbau, and Ramon Villarino, "Analysis of Vital Signs Monitoring using an IR-UWB Radar," *Progress in Electromagnetics Research*, vol. 100, pp. 265-284, 2010. [CrossRef] [Google Scholar] [Publisher Link]

[4] Antonio Lazaro, David Girbau, and Ramon Villarino, "Techniques for Clutter Suppression in the Presence of Body Movements During the Detection of Respiratory Activity through UWB Radars," *Sensors*, vol. 14, no. 2, pp. 2595-2618, 2014. [CrossRef] [Google Scholar] [Publisher Link]

[5] Marta Cavagnaro, Erika Pittella, and Stefano Pisa, "UWB Pulse Propagation into Human Tissues," *Physics in Medicine and Biology*, vol. 58, no. 24, pp. 8689-8707, 2013. [CrossRef] [Google Scholar] [Publisher Link]

[6] Mahdi Esmaeilishahir, Ali Shakfa, and Saeid Karamzadeh, "Experimental Study of Noncontact Detection of Vital Signs using IR-UWB Radar," *2023 Workshop on Microwave Theory and Technology in Wireless Communications (MTTW)*, Riga, Latvia, pp. 84-88, 2023. [CrossRef] [Google Scholar] [Publisher Link]

[7] Xiaochao Dang, Jinlong Zhang, and Zhanjun Hao, "A Noncontact Detection Method for Multi-Person Vital Signs based on IR-UWB Radar," *Sensors*, vol. 22, no. 16, pp. 1-21, 2022. [CrossRef] [Google Scholar] [Publisher Link]

[8] Lida Kouhalvandi, and Saeid Karamzadeh, "Advances in Noncontact Human Vital Sign Detection: A Detailed Survey of Radar and Wireless Solutions," *IEEE Access*, vol. 13, pp. 27833-27851, 2025. [CrossRef] [Google Scholar] [Publisher Link]

[9] Faheem Khan et al., "IR-UWB Radar-based Robust Heart Rate Detection using a Deep Learning Technique Intended for Vehicular Applications," *Electronics*, vol. 11, no. 16, pp. 1-15, 2022. [CrossRef] [Google Scholar] [Publisher Link]

[10] Zhen Yang et al., "A Method of UWB Radar Vital Detection based on P-Time Extraction of Strong Vital Signs," *Journal of Sensors*, vol. 2021, no. 1, pp. 1-10, 2021. [CrossRef] [Google Scholar] [Publisher Link]

[11] Shuaikang Xue et al., "Simultaneous Multi-Person Vital Signs Monitoring using Multiple-Input Multiple-Output FMCW Millimeter Wave Radar," *AEU - International Journal of Electronics and Communications*, vol. 188, 2025. [CrossRef] [Google Scholar] [Publisher Link]

[12] Xinyue Zhang et al., "Contactless Simultaneous Breathing and Heart Rate Detections in Physical Activity using IR-UWB Radars," *Sensors*, vol. 21, no. 16, pp. 1-18, 2021. [CrossRef] [Google Scholar] [Publisher Link]

[13] Xiuzhu Yang et al., "Body Orientation and Vital Sign Measurement with IR-UWB Radar Network," *2020 42nd Annual International Conference of the IEEE Engineering in Medicine and Biology Society (EMBC)*, Montreal, QC, Canada, pp. 485-488, 2020. [CrossRef] [Google Scholar] [Publisher Link]

[14] Huimin Yu, Wenjun Huang, and Baoqiang Du, "SSA-VMD for UWB Radar Sensor Vital Sign Extraction," *Sensors*, vol. 23, no. 2, pp. 1-14, 2023. [CrossRef] [Google Scholar] [Publisher Link]

[15] Yunnan Wu et al., "Impulse Radio Pulse Shaping for Ultra-Wide Bandwidth (UWB) Systems," *14th IEEE Proceedings on Personal, Indoor and Mobile Radio Communications, 2003. PIMRC 2003.*, Beijing, China, vol. 1, pp. 877-881, 2003. [CrossRef] [Google Scholar] [Publisher Link]

[16] Jia-hao Qiao et al., "Contactless Multiscale Measurement of Cardiac Motion using a Biomedical Radar Sensor," *Frontiers in Cardiovascular Medicine*, vol. 9, pp. 1-13, 2022. [CrossRef] [Google Scholar] [Publisher Link]

[17] Faheem Khan, and Sung Ho Cho, "A Detailed Algorithm for Vital Sign Monitoring of a Stationary/Non-Stationary Human Through IR-UWB Radar," *Sensors*, vol. 17, no. 2, pp. 1-15, 2017. [CrossRef] [Google Scholar] [Publisher Link]

[18] Wei Huang et al., "Microwave Heartprint: A Novel Noncontact Human Identification Technology based on Cardiac Micro-Motion Detection using Ultra Wideband Bio-Radar," *Journal of Bio Medical Engineering*, vol. 41, no. 2, pp. 272-280, 2024. [CrossRef] [Google Scholar] [Publisher Link]

[19] Xiaolin Liang et al., "Through-Wall Human Being Detection using UWB Impulse Radar," *EURASIP Journal on Wireless Communications and Networking*, vol. 2018, no. 1, pp. 1-17, 2018. [CrossRef] [Google Scholar] [Publisher Link]

[20] Artit Rittiplang, Pattarapong Phasukkit, and Teerapong Orankitanun, "Optimal Central Frequency for Noncontact Vital Sign Detection using Monocycle UWB Radar," *Sensors*, vol. 20, no. 10, pp. 1-19, 2020. [CrossRef] [Google Scholar] [Publisher Link]

[21] M. Ghavami, L.B. Michael, and R. Kohno, *Ultra-Wideband Signals and Systems in Communication Engineering*, John Wiley and Sons, pp. 1-27, 2007. [CrossRef] [Google Scholar] [Publisher Link]

[22] Jingwen Zhang et al., "A Multi-Target Localization and Vital Sign Detection Method using Ultra-Wide Band Radar," *Sensors*, vol. 23, no. 13, pp. 1-18, 2023. [CrossRef] [Google Scholar] [Publisher Link]

[23] Sachin Kishanrao Bhingikar, Rishi Raj Sharma, and Ram Bilas Pachor, "Radar-based Noncontact Heart Rate Monitoring: A Comprehensive Review," *Digital Signal Processing*, vol. 168, 2026. [CrossRef] [Google Scholar] [Publisher Link]

[24] Zhenzhen Duan, and Jing Liang, "Non-Contact Detection of Vital Signs using a UWB Radar Sensor," *IEEE Access*, vol. 7, pp. 36888-36895, 2019. [CrossRef] [Google Scholar] [Publisher Link]

[25] Dingyang Wang, Sungwon Yoo, and Sung Ho Cho, "Experimental Comparison of IR-UWB Radar and FMCW Radar for Vital Signs," *Sensors*, vol. 20, no. 22, pp. 1-22, 2020. [CrossRef] [Google Scholar] [Publisher Link]

[26] Hongqiang Xu et al., "Accurate Heart Rate and Respiration Rate Detection based on a Higher-Order Harmonics Peak Selection Method using Radar Noncontact Sensors," *Sensors*, vol. 22, no. 1, pp. 1-17, 2021. [CrossRef] [Google Scholar] [Publisher Link]

[27] Youngwook Kim, and Hao Ling, "Human Activity Classification based on Micro-Doppler Signatures using a Support Vector Machine," *IEEE Transactions on Geoscience and Remote Sensing*, vol. 47, no. 5, pp. 1328-1337, 2009. [CrossRef] [Google Scholar] [Publisher Link]

[28] Faheem Khan et al., "An Overview of Signal Processing Techniques for Remote Health Monitoring using Impulse Radio UWB Transceiver," *Sensors*, vol. 20, no. 9, pp. 1-21, 2020. [CrossRef] [Google Scholar] [Publisher Link]

[29] Peter Blahút, Normal Values (Echocardiography), TECHmED.sk, 2025. [Online]. Available: https://www.techmed.sk/en/echo/normal-values/

[30] Adrian Bekasiewicz et al., "Miniaturization-Oriented Design of Spline-Parameterized UWB Antenna for Indoor Positioning Applications," *International Conference on Computational Science*, Malaga, Spain, vol. 7, pp. 37-45, 2024. [CrossRef] [Google Scholar] [Publisher Link]

[31] Hesham A. Mohamed, and Mohamed Aboualalaa, "A Low-Profile Super UWB-MIMO Antenna with D-Shaped Elements for Satellite Communications, 5G and Beyond Applications," *Scientific Reports*, vol. 15, no. 1, pp. 1-19, 2025. [CrossRef] [Google Scholar] [Publisher Link]

[32] Umair Rafique et al., "Ultra-Wideband Antennas for Biomedical Imaging Applications: A Survey," *Sensors*, vol. 22, no. 9, pp. 1-38, 2022. [CrossRef] [Google Scholar] [Publisher Link]

[33] Bradley J. Roth, "Electrical Conductivity Values used with the Bidomain Model of Cardiac Tissue," *IEEE Transactions on Biomedical Engineering*, vol. 44, no. 4, pp. 326-328, 1997. [CrossRef] [Google Scholar] [Publisher Link]

[34] Niko Ištuk et al., "Dielectric Properties of Ovine Heart at Microwave Frequencies," *Diagnostics*, vol. 11, no. 3, pp. 1-15, 2021. [CrossRef] [Google Scholar] [Publisher Link]

[35] Felix Essingholt et al., "Non-Invasive Heart Beat Measurement using Microwave Resonators," *Proceedings*, vol. 2, no. 13, pp. 1-4, 2018. [CrossRef] [Google Scholar] [Publisher Link]

[36] G.K. Pandey et al., "High Gain Vivaldi Antenna for Radar and Microwave Imaging Applications," *International Journal of Signal Processing Systems*, vol. 3, no. 1, pp. 35-39, 2015. [CrossRef] [Google Scholar] [Publisher Link]